Microscopic study of the impurity effect in the kagome superconductor La(Ru$_{1-x}$Fe$_x$)$_3$Si$_2$

C. Mielke, III [1,2,*] D. Das,[1] J. Spring [2] H. Nakamura,[3] S. Shin [4] H. Liu [2] V. Sazgari [1] S. Jöhr,[2] J. Lyu,[4]
J. N. Graham,[1] T. Shiroka,[1] M. Medarde,[4] M. Z. Hasan,[5,6,7,8] S. Nakatsuji,[9,3,10,11,12] R. Khasanov,[1]
D. J. Gawryluk,[4] H. Luetkens,[1] and Z. Guguchia[1,†]

[1]*Laboratory for Muon Spin Spectroscopy, Paul Scherrer Institute, CH-5232 Villigen PSI, Switzerland*
[2]*Physik-Institut, Universität Zürich, Winterthurerstrasse 190, CH-8057 Zürich, Switzerland*
[3]*Institute for Solid State Physics (ISSP), University of Tokyo, Kashiwa, Chiba 277-8581, Japan*
[4]*Laboratory for Multiscale Materials Experiments, Paul Scherrer Institute, CH-5232 Villigen PSI, Switzerland*
[5]*Laboratory for Topological Quantum Matter and Advanced Spectroscopy (B7), Department of Physics,*
Princeton University, Princeton, New Jersey 08544, USA
[6]*Princeton Institute for the Science and Technology of Materials, Princeton University, Princeton, New Jersey 08540, USA*
[7]*Materials Sciences Division, Lawrence Berkeley National Laboratory, Berkeley, California 94720, USA*
[8]*Quantum Science Center, Oak Ridge, Tennessee 37831, USA*
[9]*Department of Physics, University of Tokyo, Bunkyo-ku, Tokyo 113-0033, Japan*
[10]*Trans-scale Quantum Science Institute, University of Tokyo, Bunkyo-ku, Tokyo 113-8654, Japan*
[11]*Institute for Quantum Matter and Department of Physics and Astronomy, Johns Hopkins University, Baltimore, Maryland 21218, USA*
[12]*Canadian Institute for Advanced Research, Toronto, Ontario M5G 1Z7, Canada*

We report on the effect of magnetic impurities on the microscopic superconducting (SC) properties of the kagome-lattice superconductor La(Ru$_{1-x}$Fe$_x$)$_3$Si$_2$ using muon spin relaxation/rotation. A strong suppression of the superconducting critical temperature T_c, the SC volume fraction, and the superfluid density was observed. We further find a correlation between the superfluid density and T_c which is considered a hallmark feature of unconventional superconductivity. Most remarkably, measurements of the temperature-dependent magnetic penetration depth λ reveal a change in the low-temperature behavior from exponential saturation to a linear increase, which indicates that Fe doping introduces nodes in the superconducting gap structure at concentrations as low as $x = 0.015$. Our results point to a rare example of unconventional superconductivity in the correlated kagome lattice and accessible tunability of the superconducting gap structure, offering new insights into the microscopic mechanisms involved in superconducting order.

I. INTRODUCTION

The unique kagome lattice, formed by an interwoven network of corner-sharing triangles, is a well-known playground for exploring the interplay between frustrated magnetism, electronic correlation, and topology [1–11]. Thanks to the natural geometrical frustration and unique electronic structure exhibiting flat bands, van Hove singularities, and Dirac nodes, kagome lattice materials can host many fascinating physical phenomena. One of the rarest phenomena experimentally observed in kagome lattice materials is superconductivity, which has a long history of theoretically predicted exotic superconducting pairings [12–15], and has been found to display competing magnetic [3,16–19] or otherwise unconventional [20–22] features. In our recent work [21] on LaRu$_3$Si$_2$, exhibiting the highest superconducting critical temperature T_c among the known bulk kagome-lattice superconductors, we found that the T_c cannot be explained solely by electron-phonon coupling. Rather, it experiences additional enhancement from typical kagome band structure features

found near the Fermi energy [21]. This manifests a superconductivity mediated primarily by electronic correlations arising from the kagome lattice, which is an unconventional superconducting order (i.e., non-BCS). The rich interplay of competing physics in kagome systems is further complicated in LaRu$_3$Si$_2$ following the recent observation of charge order (CO) at temperatures as high as 400 K [22], which adds an additional electronic correlation to the normal state of this prototypical kagome superconductor.

Following the discovery of superconductivity in LaRu$_3$Si$_2$ [23], doping and impurity effect studies were performed, first on the La site [24,25], and more recently on the Ru site [26,27]. Previous reports on the effect of substitution of the kagome-lattice-forming Ru atoms by various magnetic and nonmagnetic atoms in La(Ru$_{1-x}$A$_x$)$_3$Si$_2$ revealed that T_c is rather insensitive to the element used as a dopant (A = Co, Ni, Cr, Fe, Ir, Rh), except in the case of Fe [26–28]. Fe doping causes a dramatic suppression of T_c with a critical concentration of $x_{cr,\text{Fe}} \simeq 0.036$. Until now, the only known property of the superconducting state in La(Ru$_{1-x}$Fe$_x$)$_3$Si$_2$ is the doping-dependent evolution of T_c. In light of the recently discovered tunability of the superconducting gap structure in the AV$_3$Sb$_5$ (A = K, Rb) family [18] which marks the kagome lattice as an

───────
*charles-hillis.mielke-iii@psi.ch
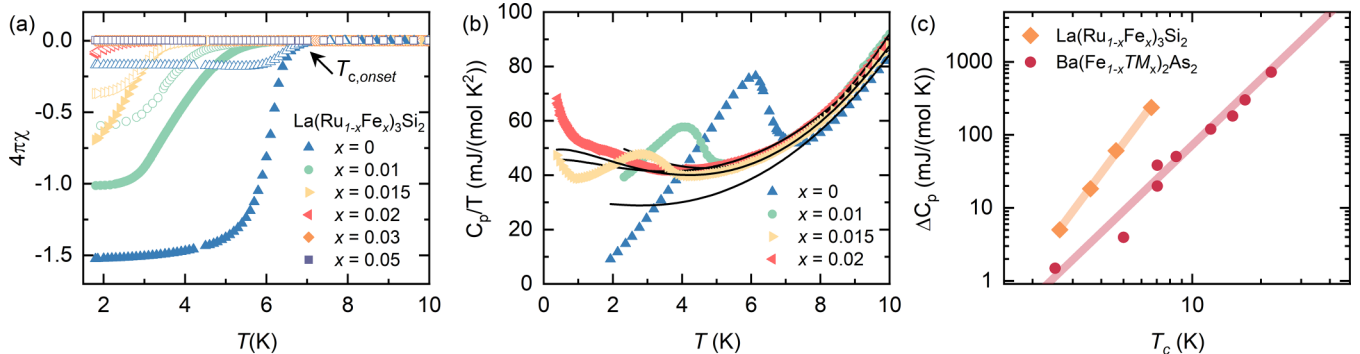†zurab.guguchia@psi.ch

FIG. 1. (a) Magnetic susceptibility vs temperature scans for an applied field of 5 mT highlighting the suppression of superconductivity with increasing Fe concentration. ZFC and FC conditions are denoted by closed and open symbols, respectively. The onset of the superconducting transition, defined as the intersection between the line tangent at the midpoint of the superconducting transition and the slope of the magnetization in the normal state, has been indicated by an arrow. (b) Sample specific heat divided by the temperature vs temperature, showing clear peaks for undoped, $x = 0.015$, and $x = 0.01$ samples and a noticeable anomaly for the $x = 0.02$ sample, which is however embedded in a large increase in C_p/T with decreasing temperature. Fits have been overlaid as solid black lines. (c) Extracted ΔC_p jump vs T_c from heat capacity measurements for each dopant concentration. Data from the current study are represented by the orange diamonds. Red triangles represent the characteristic scaling relation found for Fe-based superconductors [30]. It has been fitted with a linear relation on a logarithmic plot, giving a $T^{4.2}$ relation, notably steeper than the BNC T^3 relation. Data have been reproduced from [30].

exceptional platform to investigate competing phases and unconventional superconductivity, a microscopic understanding of the suppression of superconductivity in La(Ru$_{1-x}$Fe$_x$)$_3$Si$_2$ from both experimental and theoretical perspectives is required.

To shed light on the nature of the suppression of superconductivity in this prototypical kagome superconductor, we investigated the superconducting properties of La(Ru$_{1-x}$Fe$_x$)$_3$Si$_2$ (from $x = 0$ to $x = 0.05$) using a combination of complementary experimental methods such as heat capacity, magnetization, and muon spin relaxation/rotation (μSR). We observed that the introduction of Fe results in neither magnetic order nor a spin-glass state. At the same time, we provide microscopic evidence for highly tunable unconventional superconductivity in La(Ru$_{1-x}$Fe$_x$)$_3$Si$_2$ as evidenced by the observation of nodal superconductivity, promoted by Fe doping, and an unconventional dependence of the superfluid density on the superconducting critical temperature.

II. EXPERIMENTAL DETAILS AND RESULTS

Figure 1(a) shows the temperature dependence of magnetic susceptibility χ for polycrystalline samples of La(Ru$_{1-x}$Fe$_x$)$_3$Si$_2$ with $x = 0$, 0.01, 0.015, 0.02, 0.03, and 0.05, measured in an applied field of 5 mT in both zero-field-cooled (ZFC) and field-cooled (FC) conditions, denoted by closed and open symbols, respectively. A clear suppression of both the onset of T_c and diamagnetic screening is observed as a result of Fe doping. The sample with $x = 0.05$ shows no diamagnetic screening, while a diamagnetic screening was clearly observed in undoped and Fe-doped samples with $x = 0.01$, 0.015, and 0.02, and a very weak diamagnetic screening in the $x = 0.03$ sample starting just above 1.8 K, the lowest temperature achievable for our magnetization measurements.

In addition to diamagnetism, it is essential to check the bulk nature of superconductivity, which may be accomplished

through heat capacity measurements. The heat capacity of the undoped and Fe-doped samples with $x = 0.01$, 0.015, and 0.02 was measured and all show a peak at T_c [see Fig. 1(b)]; both the value of T_c and the height of the peak are suppressed as a result of Fe doping, indicating a reduction in superconducting volume fraction. The specific heat peak for the sample $x = 0.02$ is severely reduced. The normal state contribution was best fitted with a model accounting for electronic correlation effects present in the sample, as previously reported [29]. This equation is of the form

$$C = \gamma T + \beta T^3 - A T^n \ln T, \quad (1)$$

where γ is the Sommerfeld parameter, β represents the weight of the phonon contribution, and the last term gives the correction to the Fermi liquid description, where n indicates the strength of the correlations. In the case of a Fermi liquid with strong correlations $n = 1$, while for the case of weak correlation $n = 3$ [29]. By analyzing the normal state data in the narrow temperature range just above T_c (i.e., 3–10 K for $x = 0.02$, 5–10 K for $x = 0.015$, 5.8–10 K for $x = 0.01$, and 7–10 K for the undoped sample), we find that $n \simeq 2$. This implies that the system is moderately correlated. After subtraction of the normal state contribution, we were able to extract the jump in specific heat at T_c, which is plotted against T_c in Fig. 1(c). Here, we find a linear relation when plotted on a logarithmic scale, which indicates a power-law scaling relation $\Delta C_p \propto T_c^{4.2}$, stronger than the T_c^3 scaling found for the Fe-based superconductors shown by the so-called BNC (Bud'ko-Ni-Canfield) scaling behavior [30,31]. Additionally, the reduced peak size indicates a suppression of the superconducting volume fraction; however, the peak size in the specific heat may be affected by changes in the coupling strength or the superconducting volume fraction, while in μSR they may be extracted separately. Thus, as volume fraction is more directly probed via μSR, it will be elaborated later [see Fig. 4(a)]. It is important to note that the broadening of the peak may also be related to some inhomogeneity of iron
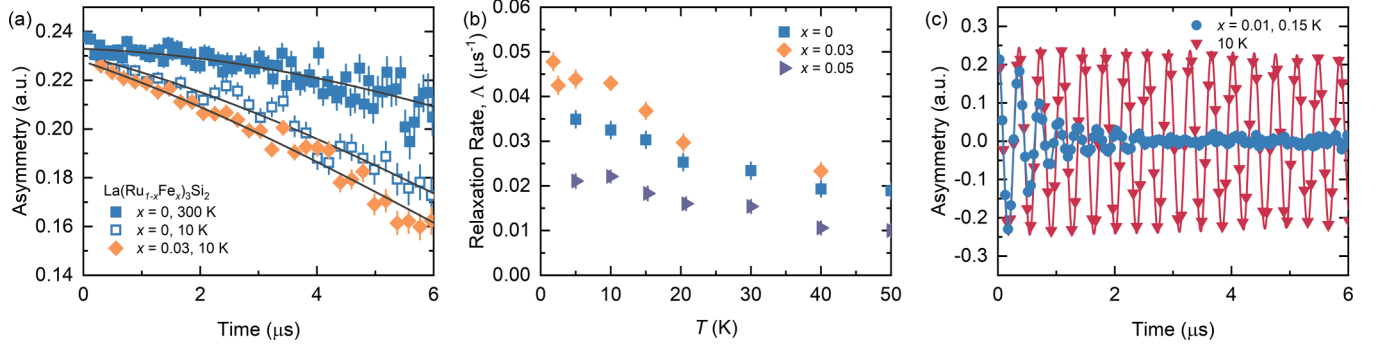
FIG. 2. (a) ZF-μSR spectra, recorded for undoped and $x = 0.03$ Fe-doped samples, at 300 K and 10 K. The black line indicates the fit to the data using Eq. (2) [32,33]. (b) Temperature dependence of the exponential relaxation rate in the undoped, $x = 0.03$, and $x = 0.05$ Fe-doped samples. The Gaussian Kubo-Toyabe was fitted with a global Δ_{GKT} parameter for each dopant concentration, which all refined to similar values (0.04–0.05 μs^{-1}). (c) Characteristic μSR time spectra for the $x = 0.01$ Fe-doped sample under 20 mT applied field in the normal state (at 10 K; red points) and in the superconducting state (at 0.15 K; blue points). Fits are shown as solid lines. The Fourier transformations showing field distribution can be found in the Supplemental Material [34].

doping. While there may be some distribution in iron doping, it should be distributed around some central value correlated to the nominal doping concentration. We also observe a smooth and linear evolution of superconducting properties with nominal doping concentration, indicative of the efficacy of doping. The fact that electronic correlation effects must be accounted for to fully reproduce the electronic specific heat is in line with the electronic-correlation-mediated superconductivity found in the parent material by band structure calculations [21]. By combining the results of the magnetization and specific heat experiments, we conclude that both T_c and the superconducting (SC) volume fraction are suppressed with increasing Fe concentration.

Next, in order to identify any potential magnetic phase or ordering which may be introduced by Fe doping, zero-field μSR experiments were performed on undoped and Fe-doped samples with $x = 0.03$ and 0.05 down to 5 K. Magnetism, if present in the samples, may enhance the muon depolarization rate in the superconducting state and falsify the interpretation of μSR results in the superconducting state. Figure 2(a) displays the zero-field μSR spectra for the samples $x = 0$ and 0.03. The ZF-μSR spectra are characterized by a weak depolarization of the muon spin ensemble and show no evidence of either long-range-ordered magnetism or a spin-glass state in La(Ru$_{1-x}$Fe$_x$)$_3$Si$_2$. The muon spin relaxation can be fully decoupled by the application of a weak longitudinal field (LF-μSR) of 5 mT (see Supplemental Material [34]), indicating that moments are static on the microsecond timescale. The ZF-μSR asymmetry spectra were fitted with a Gaussian Kubo-Toyabe function multiplied by an exponential relaxation rate as follows:

$$A(t) = A_0 \left[\frac{1}{3} + \frac{2}{3}[1 - (\Delta_{\mathrm{GKT}}t)^2]e^{-\frac{1}{2}(\Delta_{\mathrm{GKT}}t)^2} \right]e^{-\Lambda t}, \quad (2)$$

where $A(t)$ is the sample asymmetry with respect to time, A_0 is the initial asymmetry, Δ_{GKT} is the Gaussian Kubo-Toyabe relaxation rate, and Λ is the exponential relaxation rate [32,33]. The Gaussian Kubo-Toyabe function reproduces the relaxation from a dense array of nuclear moments felt by

the muon ensemble, while the exponential relaxation rate can be associated with the contribution of electronic origin. The Δ_{GKT} parameter was refined as a global parameter for each sample, and the exponential relaxation rate was allowed to vary. Δ_{GKT} converged to a similar value for all three samples ($\Delta_{\mathrm{GKT}} \simeq 0.04$ μs^{-1}), indicating that the nuclear moments which contribute to the Gaussian Kubo-Toyabe relaxation rate remain similar across the doping series. The temperature dependence of the exponential relaxation rate is shown in Fig. 2(b) for the undoped and $x = 0.03$, 0.05 samples. There is only a small increase in the normal state muon-spin relaxation rate at low temperatures, which is present in the undoped as well as the Fe-doped samples. The nonmonotonic dependence of the baseline and the increase in relaxation rate with decreasing temperatures deserve further attention, especially following the discovery of a high-temperature charge-ordered state [22], and will be the subject of future studies. Thus, the current results show that introducing a small amount of Fe in La(Ru$_{1-x}$Fe$_x$)$_3$Si$_2$ does not introduce any additional magnetic state not already present in the parent compound.

Once it was established that no enhancement of muon depolarization rate was introduced by Fe doping, the suppression of the superconducting state could be explored microscopically using transverse field (TF) μSR. We probe the SC order parameter via the superfluid density $\sigma_{\mathrm{SC}} \propto \frac{1}{\lambda^2} \propto n_s$, where σ_{SC} is the superconducting muon spin depolarization rate. The absence of long-range magnetic order or a spin-glass state in La(Ru$_{1-x}$Fe$_x$)$_3$Si$_2$ implies that the increase of the TF relaxation rate below T_c is attributed entirely to the vortex lattice. As an example, the TF-μSR spectra for the $x = 0.01$ sample, measured in an applied magnetic field of 20 mT above (10 K) and below (0.15 K) the SC transition temperature T_c, are shown in Fig. 2(c). Above T_c the oscillations show a small relaxation rate σ_{nm} due to the random local fields from the nuclear magnetic moments. At 0.15 K, the relaxation rate increases due to the presence of a nonuniform local field distribution as a result of the formation of a flux-line lattice (FLL) in the SC state (see the Supplemental Material [34], as well as Refs. [32,37,39,40] therein). The base-T value
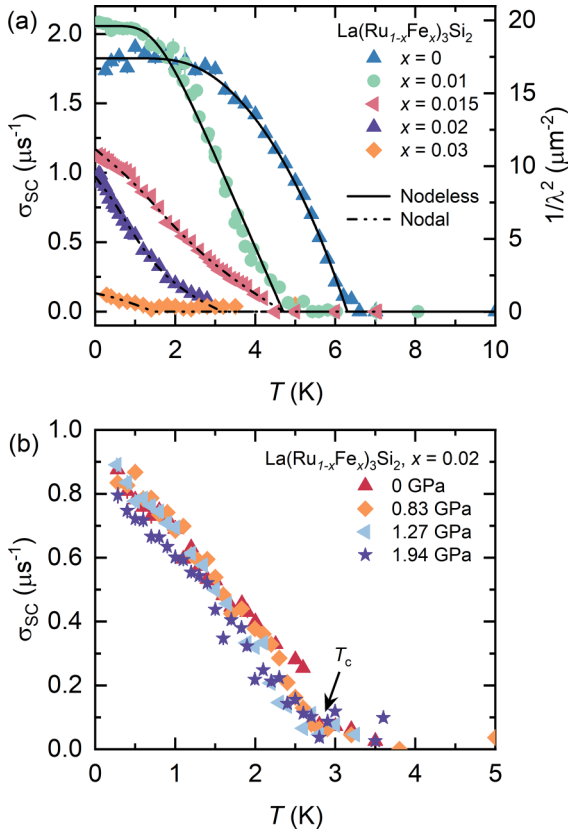
FIG. 3. (a) The temperature dependence of the superconducting muon-spin depolarization rate σ_{SC} (left axis) and the superfluid density (i.e., $\frac{1}{\lambda^2}$) (right axis) for all doped samples including the undoped polycrystalline sample, taken from [21]. The solid (dashed) lines correspond to fits using a model with nodeless (nodal) gap superconductivity. (b) Temperature dependence of σ_{SC} for the $x = 0.02$ Fe-doped sample under various applied hydrostatic pressures. The arrow indicates T_c, which remains unchanged under pressure.

of the superfluid density increases for the $x = 0.01$ sample, before decreasing rapidly for $x = 0.015$, $x = 0.02$, and $x = 0.03$ samples [see Fig. 3(a)]. Despite the nonmonotonic behavior in superfluid density, the T_c decreases monotonically with increasing Fe-dopant concentration [doping evolution of T_c is plotted in Fig. 4(a)]. We also find a constant decrease in SC volume fraction with increased doping concentration which perfectly follows the $\frac{T_c}{T_{c,\,pure}}$ dependence at low concentrations before diverging at $x = 0.015$, $x = 0.02$, and $x = 0.03$; see Fig. 4(a).

More importantly, the temperature dependence of the superfluid density suggests a change in the SC gap structure: in undoped and $x = 0.01$ samples, the temperature dependence of the superfluid density $n_s \propto \frac{1}{\lambda^2} \propto \sigma_{SC}$ saturates below $\simeq 2\,\mathrm{K}$ and 1.5 K, respectively, and has been well modeled with the s-wave superconducting gap symmetry [21]. In contrast, in the $x = 0.015$, $x = 0.02$, and $x = 0.03$ samples, the dependence of σ_{SC} increases linearly with decreasing temperature, indicating the presence of a SC gap which has nodes. This points toward a crossover from fully gapped to nodal SC gap structure with increasing Fe-dopant concentration. The introduction of Fe doping seems to have the inverse effect of hydrostatic pressure on other kagome superconductors such as KV_3Sb_5 and RbV_3Sb_5 [18], which exhibit a nodal SC gap symmetry under ambient conditions and become fully gapped under hydrostatic pressure.

The nodal superconducting state introduced by Fe doping is remarkably stable, demonstrated by additional μSR studies under pressure. The application of hydrostatic pressures up to 2 GPa was achieved, and the temperature dependence of σ_{SC} for $x = 0.02$ showed no saturation down to the lowest temperatures [see Fig. 3(b)]. In fact, the data for all four pressures probed by μSR nearly perfectly overlap, as seen in Fig. 3(b). This implies that the application of hydrostatic pressure has almost no effect on the superfluid density or T_c in the full
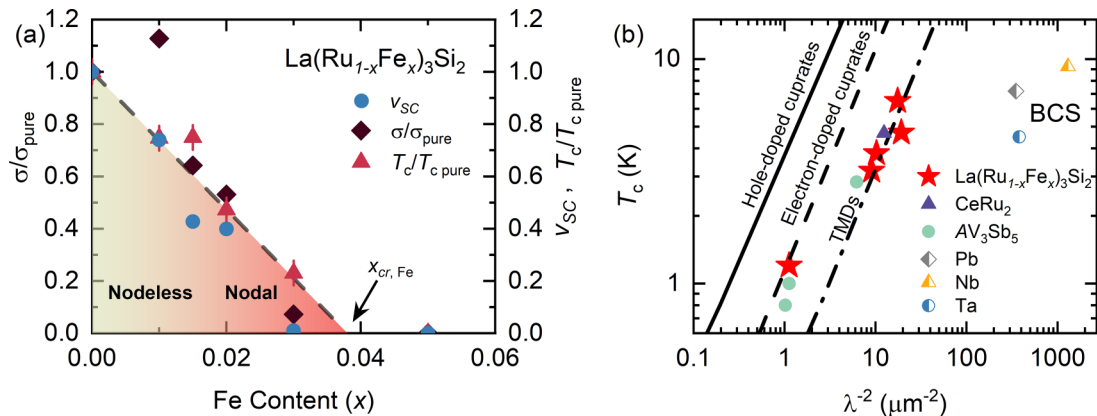

FIG. 4. (a) The doping evolution of the superconducting muon-spin depolarization rate σ_{SC}, normalized superconducting T_c, and superconducting volume fraction V_{SC}, extracted from the μSR results. The light green–to–red shaded region indicates the crossover around $x = 0.015$ from nodeless superconducting gap structure (light green) to a nodal structure (red). (b) The T_c vs superfluid density ratio has been plotted for the different dopant concentrations of $La(Ru_{1-x}Fe_x)_3Si_2$ compared with other known conventional and unconventional superconductors [18,43–47]. While all dopant concentrations lie far from the elemental conventional superconductors, they fall almost entirely along the same line as several example transition metal dichalcogenides [46,47] and other kagome superconductors [18]. Only the 3% Fe-doped sample falls a bit away from this line, and falls instead on the same line as the electron-doped cuprates, similarly to RbV_3Sb_5 and KV_3Sb_5 under ambient pressure.

pressure range, much like in the parent compound $LaRu_3Si_2$ [21]. This indicates that nodal superconductivity is the energetically preferred ground state at $x = 0.015$, $x = 0.02$, and $x = 0.03$ concentrations.

From the μSR measurements, we are able to construct the phase diagram with respect to doping concentration, which is shown in Fig. 4(a). We observe a nonmonotonic behavior of the superfluid density with Fe doping, while simultaneously identifying a continuous decrease of superconducting T_c with Fe dopant concentration. Thus we find that superconductivity is suppressed steadily from three different directions: in terms of T_c, volume fraction, and superfluid density. The anomalous increase of 20% in superfluid density at $x = 0.01$ Fe-doping concentration stands out, however. In the context of other superconductors [43–45], we see in Fig. 4(b) that the T_c and superfluid density (i.e., $\frac{1}{\lambda^2}$) values place the undoped and Fe-doped samples with $x = 0.01$, $x = 0.015$, and $x = 0.02$ all neatly along the line formed by other kagome systems [18] such as $CeRu_2$ and CsV_3Sb_5 as well as moderately correlated quasi-2D transition metal dichalcogenides (TMDs) [46,47]. This suggests a universal scaling relation common among the kagome superconductors, similar to that found in TMDs as well. The data point for the $x = 0.03$ sample lies near KV_3Sb_5 and RbV_3Sb_5 and on the same line as electron-doped cuprates, but all members in this doping series lie far from the conventional superconductors and show correlation between the superfluid density and T_c, which is considered a hallmark feature of unconventional superconductivity.

III. DISCUSSION

There is a long history of predicting [12–14] different types of electronic instabilities on the kagome lattices at select fillings (e.g., 5/4 electrons per band) such as charge density wave order, bond density wave state, chiral spin density wave states, and superconductivity with $d + id$- or f-wave superconductivity. The experimental realization of these exotic superconducting pairings has been largely missing until recently, following the discovery of the AV_3Sb_5 (A = K, Rb, Cs) family, which has unleashed an avalanche of interest in kagome systems. A nodal superconducting pairing has been found experimentally in KV_3Sb_5 and RbV_3Sb_5, and can be tuned to nodeless s-wave symmetry by the application of hydrostatic pressure [18] and by doping [48]. The crossover from nodal to nodeless pairing is correlated with the establishment of the optimal superconducting region of the phase diagram, which corresponds to full suppression of charge order in KV_3Sb_5 and partial suppression of charge order in RbV_3Sb_5. The essential findings of this paper are the observation of the unconventional scaling of the superfluid density with respect to T_c, and the crossover from nodeless to a superconducting gap structure with nodes, promoted by Fe doping in $La(Ru_{1-x}Fe_x)_3Si_2$. Thus, in the present case of $La(Ru_{1-x}Fe_x)_3Si_2$, we have uncovered yet another highly tunable unconventional kagome superconductor, and are able to introduce nodes in the superconducting gap structure with the introduction of a small quantity of Fe doping without introducing a competing magnetic state. It is furthermore interesting to note that a high-temperature charge order has been uncovered in the $La(Ru_{1-x}Fe_x)_3Si_2$ system [22]; however, the

onset temperature lies around 400 K in the parent, undoped compound $LaRu_3Si_2$, which exhibits nodeless superconductivity and a $T_c = 7$ K [21], similar to CsV_3Sb_5 once charge order has been fully suppressed [19]. Therefore, it seems that the Fe doping causes the changes in the Fermi surface without the presence of a competing state. Whether the SC gap topology is well ordered (i.e., d-wave superconductivity, where the nodes occur at $\frac{\pi}{2}$ spacing) or the nodes are "accidental" [35,36] is difficult to determine with μSR. Further investigations are desirable to distinguish between the two.

IV. CONCLUSION

In conclusion, we have studied the effect of Fe doping on the superconducting and normal state properties of the prototypical kagome superconductor $LaRu_3Si_2$. The introduction of iron on the ruthenium site neither precipitates a magnetic state with long-range order nor introduces a novel magnetic state not already present in the parent compound. However, we have observed a strong suppression of superconductivity, which is manifested by the suppression of the volume fraction, suppression of T_c, and suppression of the superfluid density. We further show an unconventional dependence of the superfluid density on the superconducting critical temperature. Most importantly, we find a crossover from fully gapped superconductivity in the parent compound to a superconductivity with nodes by $x = 0.015$ Fe substitution, less than half the critical doping concentration required to fully suppress superconductivity. This study will serve to stimulate useful discussion regarding the nature of kagome superconductivity and the delicate balance it holds between competing orders.

[1] Z. Guguchia, J. Verezhak, D. Gawryluk, S. Tsirkin, J.-X. Yin, I. Belopolski, H. Zhou, G. Simutis, S.-S. Zhang, T. Cochran *et al.*, Tunable anomalous Hall conductivity through volume-wise magnetic competition in a topological kagome magnet, Nat. Commun. **11**, 559 (2020).

[2] J.-X. Yin, S. Zhang, H. Li, K. Jiang, G. Chang, B. Zhang, B. Lian, C. Xiang, I. Belopolski, H. Zheng *et al.*, Giant and anisotropic spin-orbit tunability in a strongly correlated kagome magnet, Nature (London) **562**, 91 (2018).

[3] C. Mielke III, D. Das, J.-X. Yin, H. Liu, R. Gupta, Y.-X. Jiang, M. Medarde, X. Wu, H. Lei, J. Chang *et al.*, Time-reversal symmetry-breaking charge order in a kagome superconductor, Nature (London) **602**, 245 (2022).

[4] K. Jiang, T. Wu, J.-X. Yin, Z. Wang, M. Z. Hasan, S. D. Wilson, X. Chen, and J. Hu, Kagome superconductors AV_3Sb_5 (A = K, Rb, Cs), Nat. Sci. Rev. **10**, nwac199 (2023).

[5] T. Neupert, M. M. Denner, J.-X. Yin, R. Thomale, and M. Z. Hasan, Charge order and superconductivity in kagome materials, Nat. Phys. **18**, 137 (2022).

[6] C. Mielke III, W. Ma, V. Pomjakushin, O. Zaharko, S. Sturniolo, X. Liu, V. Ukleev, J. White, J.-X. Yin, S. Tsirkin *et al.*, Low-temperature magnetic crossover in the topological kagome magnet $TbMn_6Sn_6$, Commun. Phys. **5**, 107 (2022).

[7] B. R. Ortiz, S. M. L. Teicher, Y. Hu, J. L. Zuo, P. M. Sarte, E. C. Schueller, A. M. Milinda Abeykoon, M. J. Krogstad, S. Rosenkranz, R. Osborn, R. Seshadri, L. Balents, J. He, and S. D. Wilson, CsV_3Sb_5: A $\mathbb{Z}_2$ topological kagome metal with a superconducting ground state, Phys. Rev. Lett. **125**, 247002 (2020).

[8] Y.-X. Jiang, J.-X. Yin, M. Denner, N. Shumiya, B. Ortiz, G. Xu, Z. Guguchia, J. He, M. Hossain, X. Liu *et al.*, Unconventional chiral charge order in kagome superconductor KV_3Sb_5, Nat. Mater. **20**, 1353 (2021).

[9] J.-X. Yin, B. Lian, and M. Z. Hasan, Topological kagome magnets and superconductors, Nature (London) **612**, 647 (2022).

[10] N. Ghimire and I. Mazin, Topology and correlations on the kagome lattice, Nat. Mater. **19**, 137 (2020).

[11] L. Ye, M. Kang, J. Liu, F. von Cube, C. Wicker, T. Suzuki, C. Jozwiak, A. Bostwick, E. Rotenberg, D. Bell *et al.*, Massive Dirac fermions in a ferromagnetic kagome metal, Nature (London) **555**, 638 (2018).

[12] M. Kiesel, C. Platt, and R. Thomale, Unconventional Fermi surface instabilities in the kagome Hubbard model, Phys. Rev. Lett. **110**, 126405 (2013).

[13] Y.-P. Lin and R. Nandkishore, Complex charge density waves at Van Hove singularity on hexagonal lattices: Haldane-model phase diagram and potential realization in the kagome metals AV_3Sb_5 (A = K, Rb, Cs), Phys. Rev. B **104**, 045122 (2021).

[14] W.-S. Wang, Z.-Z. Li, Y.-Y. Xiang, and Q.-H. Wang, Competing electronic orders on kagome lattices at van Hove filling, Phys. Rev. B **87**, 115135 (2013).

[15] C. Setty, H. Hu, L. Chen, and Q. Si, Electron correlations and T-breaking density wave order in a Z_2 kagome metal, arXiv:2105.15204.

[16] C. Mielke III, H. Liu, D. Das, J.-X. Yin, L. Deng, J. Spring, R. Gupta, M. Medarde, C.-W. Chu, R. Khasanov *et al.*, Local spectroscopic evidence for a nodeless magnetic kagome superconductor CeRu$_2$, J. Phys.: Condens. Matter **34**, 485601 (2022).

[17] R. Khasanov, D. Das, R. Gupta, C. Mielke III, M. Elender, Q. Yin, Z. Tu, C. Gong, H. Lei, E. T. Ritz, R. M. Fernandes, T. Birol, Z. Guguchia, and H. Luetkens, Time reversal symmetry broken by charge order in CsV_3Sb_5, Phys. Rev. Res. **4**, 023244 (2022).

[18] Z. Guguchia, C. Mielke III, D. Das, R. Gupta, J.-X. Yin, H. Liu, Q. Yin, M. Christensen, Z. Tu, C. Gong *et al.*, Tunable unconventional kagome superconductivity in charge ordered RbV_3Sb_5 and KV_3Sb_5, Nat. Commun. **14**, 153 (2023).

[19] R. Gupta III, D. Das, C. Mielke III, E. Ritz, F. Hotz, Q. Yin, Z. Tu, C. Gong, H. Lei, T. Birol *et al.*, Two types of charge order with distinct interplay with superconductivity in the kagome material CsV_3Sb_5, Commun. Phys. **5**, 232 (2022).

[20] R. Gupta, D. Das, C. Mielke III, Z. Guguchia, T. Shiroka, C. Baines, M. Bartkowiak, H. Luetkens, R. Khasanov, Q. Yin *et al.*, Microscopic evidence for anisotropic multigap superconductivity in the CsV_3Sb_5 kagome superconductor, npj Quantum Mater. **7**, 49 (2022).

[21] C. Mielke III, Y. Qin, J.-X. Yin, H. Nakamura, D. Das, K. Guo, R. Khasanov, J. Chang, Z. Q. Wang, S. Jia, S. Nakatsuji, A. Amato, H. Luetkens, G. Xu, M. Z. Hasan, and Z. Guguchia, Nodeless kagome superconductivity in $LaRu_3Si_2$, Phys. Rev. Mater. **5**, 034803 (2021).

[22] I. Plokhikh, C. Mielke III, H. Nakamura, V. Petricek, Y. Qin, V. Sazgari, J. Küspert, I. Bialo, S. Shin, O. Ivashko *et al.*, Charge order above room-temperature in a prototypical kagome superconductor La$(Ru_{1-x}Fe_x)_3Si_2$, arXiv:2309.09255.

[23] H. Barz, New ternary superconductors with silicon, Mater. Res. Bull. **15**, 1489 (1980); J. M. Vandenberg and H. Barz, The crystal structure of a new ternary silicide in the system rare-earth-ruthenium-silicon, *ibid.* **15**, 1493 (1980).

[24] C. Godart and L. Gupta, Coexistence of superconductivity and spin glass freezing in $La_{0.95}Gd_{0.05}Ru_3Si_2$, Phys. Lett. A **120**, 427 (1987).

[25] M. Escorne, A. Mauger, L. Gupta, and C. Godart, Type-II superconductivity in a dilute magnetic system: $La_{1-x}Tm_xRu_3Si_2$, Phys. Rev. B **49**, 12051 (1994).

[26] S. Li, J. Tao, X. Wan, X. Ding, H. Yang, and H.-H. Wen, Distinct behaviors of suppression to superconductivity in $LaRu_3Si_2$ induced by Fe and Co dopants, Phys. Rev. B **86**, 024513 (2012).

[27] B. Li, S. Li, and H.-H. Wen, Chemical doping effect in the $LaRu_3Si_2$ superconductor with a kagome lattice, Phys. Rev. B **94**, 094523 (2016).

[28] S. Chakrabortty, R. Kumar, and N. Mohapatra, Effect of tunable spin-orbit coupling on the superconducting properties of $LaRu_3Si_2$ containing kagome-honeycomb layers, Phys. Rev. B **107**, 024503 (2023).

[29] S. Li, B. Zeng, X. Wan, J. Tao, F. Han, H. Yang, Z. Wang, and H.-H. Wen, Anomalous properties in the normal and superconducting states of $LaRu_3Si_2$, Phys. Rev. B **84**, 214527 (2011).

[30] Z. Guguchia, R. Khasanov, Z. Bukowski, F. von Rohr, M. Medarde, P. K. Biswas, H. Luetkens, A. Amato, and E. Morenzoni, Probing the pairing symmetry in the over-doped Fe-based superconductor $Ba_{0.35}Rb_{0.65}Fe_2As_2$ as a function of hydrostatic pressure, Phys. Rev. B **93**, 094513 (2016).

[31] S. Bud'ko, N. Ni, and P. Canfield, Jump in specific heat at the superconducting transition temperature in $Ba(Fe_{1-x}Co_x)_2As_2$ and $Ba(Fe_{1-x}Ni_x)_2As_2$ single crystals, Phys. Rev. B **79**, 220516(R) (2009).

[32] A. Suter and B. M. Wojek, Musrfit: A free platform-independent framework for μSR data analysis, Phys. Procedia **30**, 69 (2012).

[33] R. Kubo and T. Toyabe, *Magnetic Resonance and Relaxation* (North Holland, Amsterdam, 1967).

[34] See Supplemental Material at http://link.aps.org/supplemental/10.1103/PhysRevB.109.134501 for details related to synthesis, magnetization, heat capacity, and μSR experiments, as well as the fitting procedures and parameters. It includes Refs. [26,27,29,32,35,37–48].

[35] Z. Guguchia, A. Amato, J. Kang, H. Luetkens, P. K. Biswas, G. Prando, F. von Rohr, Z. Bukowski, A. Shengelaya, H. Keller *et al.*, Direct evidence for the emergence of a pressure induced nodal superconducting gap in the iron-based superconductor $Ba_{0.65}Rb_{0.35}Fe_2As_2$, Nat. Commun. **6**, 8863 (2015).

[36] S. Maiti, R. Fernandes, and A. Chubukov, Gap nodes induced by coexistence with antiferromagnetism in iron-based superconductors, Phys. Rev. B **85**, 144527 (2012).

[37] E. H. Brandt, Flux distribution and penetration depth measured by muon spin rotation in high-T_c superconductors, Phys. Rev. B **37**, 2349 (1988).

[38] J. E. Sonier, J. H. Brewer, and R. F. Kiefl, μSR studies of the vortex state in type-II superconductors, Rev. Mod. Phys. **72**, 769 (2000).

[39] M. Tinkham, *Introduction to Superconductivity* (Krieger Publishing Company, Malabar, FL, 1975).

[40] A. Carrington and F. Manzano, Magnetic penetration depth of MgB_2, Phys. C (Amsterdam, Neth.) **385**, 205 (2003).

[41] J. Rodríguez-Carvajal, Recent advances in magnetic structure determination by neutron powder diffraction, Phys. B (Amsterdam, Neth.) **192**, 55 (1993).

[42] T. Shang, A. Amon, D. Kasinathan, W. Xie, M. Bobnar, Y. Chen, A. Wang, M. Shi, M. Medarde, H. Yuan, and T. Shiroka, Enhanced T_c and multiband superconductivity in the fully-gapped $ReBe_{22}$ superconductor, New J. Phys. **21**, 073034 (2019).

[43] Y. J. Uemura, G. M. Luke, B. J. Sternlieb, J. H. Brewer, J. F. Carolan, W. N. Hardy, R. Kadono, J. R. Kempton, R. F. Kiefl, S. R. Kreitzman, P. Mulhern, T. M. Riseman, D. L. Williams, B. X. Yang, S. Uchida, H. Takagi, J. Gopalakrishnan, A. W. Sleight, M. A. Subramanian, C. L. Chien, M. Z. Cieplak, G. Xiao, V. Y. Lee, B. W. Statt, C. E. Stronach, W. J. Kossler, and X. H. Yu, Universal correlations between T_c and n_s/m^* (carrier density over effective mass) in high-T_c cuprate superconductors, Phys. Rev. Lett. **62**, 2317 (1989).

[44] Y. Uemura, A. Keren, L. Le, G. Luke, B. Sternlieb, W. Wu, J. Brewer, R. Whetten, S. Huang, S. Lin *et al.*, Magnetic-field penetration depth in K_3C_{60} measured by muon spin relaxation, Nature (London) **352**, 605 (1991).

[45] A. Shengelaya, R. Khasanov, D. Eshchenko, D. Di Castro, I. Savić, M. Park, K. Kim, S.-I. Lee, K. Müller, and H. Keller, Muon-spin-rotation measurements of the penetration depth of the infinite-layer electron-doped $Sr_{0.9}La_{0.1}CuO_2$ cuprate superconductor, Phys. Rev. Lett. **94**, 127001 (2005).

[46] Z. Guguchia, F. von Rohr, Z. Shermadini, A. Lee, S. Banerjee, A. Wieteska, C. Marianetti, B. Frandsen, H. Luetkens, Z. Gong *et al.*, Signatures of the topological s^{+-} superconducting order parameter in the type-II Weyl semimetal T_d-$MoTe_2$, Nat. Commun. **8**, 1082 (2017).

[47] F. O. von Rohr, J.-C. Orain, R. Khasanov, C. Witteveen, Z. Shermadini, A. Nikitin, J. Chang, A. Wieteska, A. N. Pasupathy, M. Z. Hasan *et al.*, Unconventional scaling of the superfluid density with the critical temperature in transition metal dichalcogenides, Sci. Adv. **5**, eaav8465 (2019).

[48] Y. Zhong, J. Liu, X. Wu, Z. Guguchia, J.-X. Yin, A. Mine, Y. Li, S. Najafzadeh, D. Das, C. Mielke III *et al.*, Nodeless electron pairing in CsV_3Sb_5-derived kagome superconductors, Nature (London) **617**, 488 (2023).